RSC Advances

Dynamic Article Links ►

SAND2015-1385J

Cite this: DOI: 10.1039/c0xx00000x

www.rsc.org/xxxxxx

ARTICLE TYPE

Interaction of Cesium Adatoms with Free-Standing Graphene and Graphene-Veiled SiO_2 Surfaces

Philippe F. Weck*[a], Eunja Kim[b] and Grant W. Biedermann[a]

Received (in XXX, XXX) Xth XXXXXXXXX 20XX, Accepted Xth XXXXXXXXX 20XX

DOI: 10.1039/b000000x

The interaction of Cs adatoms with mono- or bi-layered graphene (MLG and BLG), either free-standing or on SiO_2 substrate, was investigated using density functional theory. The most stable adsorption sites for Cs are found to be hollow sites on both graphene sheets and graphene-veiled SiO_2(0001). Larger dipole moments are created when a MLG-veiled SiO_2(0001) substrate is used for adsorption of Cs atoms compared to the adsorption on free-standing MLG, due to charge transfer occurring between the MLG and the SiO_2 substrate. For the adsorption of Cs on BLG-veiled SiO_2(0001) substrate, these differences are smoothed out and the binding energies corresponding to different sites are nearly degenerate; smaller dipole moments created by the Cs adatoms on BLG compared to MLG are also predicted.

1 Introduction

The adsorption of alkali-metal (AM) atoms on surfaces has been extensively studied since the seminal work of Langmuir[1,2] and Gurney.[3] Due to the simple electronic structure of AM atoms, AM atoms–surfaces often serve as prototypical systems to gain fundamental understanding of chemisorption mechanisms, polarization, and van der Waals, Casimir-Polder and Casimir forces.[4,5] These systems also find widespread technological applications in the traditional fields of electrochemistry or heterogeneous catalysis, and have become increasingly appealing for the development of nanodevices for high-sensitivity interferometry, precision force measurements, or quantum information.[6,7,8]

However, the practical realization of such AM-containing nanodevices with satisfactory signal-to-noise performance has been hindered by motional heating in micro-fabricated traps. The experimental spectra over the observed range of frequencies suggest a $1/f$ variation with frequency and are consistent with a d^{-4} scaling, where d is the trap-surface distance, for a large variety of trapping geometries. This anomalous noise-induced heating contrasts with the most common noise source in conductors, the Johnson-Nyquist noise from the trap components, that is characterized by a frequency independent spectrum and decays as d^{-2} with increasing trap-surface distance. Recent theoretical research efforts have focused on the development of a microscopic model for this excess electric field noise, which points a way towards a more systematic understanding of surface adsorbates as progenitors of electric field jitter.[9,10]

One of the current strategies to limit or suppress this $1/f$ noise in nanodevices consists in stacking graphene monolayers with the natural graphite order on an insulating substrate.[11] Silicon dioxide (SiO_2) is widely utilized as a dielectric substrate in nanodevices and exfoliated graphene deposition on SiO_2 or direct production of graphene on SiO_2 by chemical vapour deposition were recently demonstrated.[1213,14] A limited number of first-principles studies of monolayer graphene (MLG) and bilayer graphene (BLG) on SiO_2 substrate were also reported and focused on the perturbation of the graphene band structure by the oxide substrate.[15,16,17,18]

While the adsorption of AM on graphitic systems has been the subject of active experimental and computational research,[19] no study has been carried out on the interaction of AM adatoms with MLG or BLG on SiO_2 substrate, to the best of our knowledge.

In this study, atomistic models with the framework of density functional theory (DFT) are used to investigate the interaction of Cesium atoms – envisioned for use in micro-fabricated traps – with graphene and graphene-veiled SiO_2. Since existing experimental results for Cs on graphite are somewhat controversial,[19] computational models are used to initially study the interactions of Cs atoms with free-standing MLG and BLG. These models are then extended to investigate the adsorption of Cs atoms on graphene-veiled SiO_2. Particular attention is dedicated to the change in work function as a result of Cs adsorption and associated with the creation of adatom-surface dipole moments; the fluctuation of such surface dipoles was demonstrated to be responsible for the anomalous noise-induced heating in microtraps.[9,10]

Details of the computational approach used are given in the next section, followed by a summary of our results and discussion.

2 Computational Methods

Total-energy calculations were performed using the spin-polarized density functional theory as implemented in the Vienna Ab initio Software Package (VASP).[20] The exchange correlation energy was calculated using the local density approximation (LDA) with local Perdew-Wang correlation (PWC).[21] The generalized gradient approximation with the parameterizations of

Perdew, Burke, and Ernzerhof[22] (PBE) and Perdew *et al.*[23] (PW91) were also used for MLG in order to test the sensitivity of structural parameters and work function with respect to the functionals.

The interaction between valence electrons and ionic cores was described by the projector augmented wave (PAW) method.[24,25] The Cs ($5s^2$,$5p^6$,$6s^1$), Si ($3s^2$,$3p^2$), C ($2s^2$,$2p^2$), and O ($2s^2$,$2p^4$) electrons were treated explicitly as valence electrons in the Kohn-Sham (KS) equations and the remaining cores were represented by PAW pseudopotentials. The KS equations were solved using the blocked Davidson iterative matrix diagonalization scheme[26] followed by the residual vector minimization method. The plane-wave cutoff energy for the electronic wavefunctions was set to 500 eV, ensuring the total energy of the system to be converged to within 1 meV/atom.

All structures were optimized with periodic boundary conditions applied using the conjugate gradient method, accelerated using the Methfessel-Paxton Fermi level smearing[27] with a width of 0.1 eV. The total energy of the system and Hellmann-Feynman forces acting on atoms were calculated with convergence tolerances set to 10^{-3} eV and 0.01 eV/Å, respectively. Structural optimizations and properties calculations were carried out using the Monkhorst-Pack special *k*-point scheme[28] with 5×5×5 and 5×5×1 meshes for integrations in the Brillouin zone (BZ) of bulk and slab systems, respectively.

The supercells for MLG and BLG models had a (2×2) mesh unit with a *ca.* 20.00 Å vacuum separating periodic slabs; the BLG model used a Bernal stacking (i.e. *ABAB*) similar to graphite. (2×2) graphene supercells were chosen in order to lead to a periodically repeated geometry for graphene placed on SiO_2(0001) surface. O- and Si-terminated SiO_2(0001) surfaces were built by cleaving the relaxed bulk structure of α-quartz and consisted of 5 and 6 bilayer of SiO_2, with the back side of the slabs passivated by addition of hydrogen atoms. In the structural optimization calculations, only the top two SiO_2 bilayers were allowed to relax. Although a large vacuum region of *ca*. 20 Å was used between periodic slabs, the creation of dipoles upon adsorption of atoms on only one side of the slab can lead to spurious interactions between the dipoles of successive slabs. In order to circumvent this problem, a dipole correction was applied by means of a dipole layer placed in the vacuum region following the method outlined by Neugebauer and Scheffler.[29] MLG and BLG were then placed on top of the O-terminated SiO_2(0001) surface and further optimization of these structures was carried out before studying the adsorption of Cs on their surface.

Since we are ultimately interested in the evaluating the dipole fluctuation spectrum and thereby the corresponding heating rate upon adsorption of Cs atoms onto the surface, a first step towards this goal is to assess the change in the surface electric dipole caused by adsorption of Cs adatoms. This can be tracked by calculating the change of the work function upon atomic adsorption, $\Delta W = W_{clean} - W_{ads}$, where W_{ads} and W_{clean} correspond to the values of the work function for a surface with and without atoms adsorbed, respectively. The work function, W, is defined as the minimum energy required to remove an electron from a solid to the vacuum region in the vicinity of the solid surface and is given by:

$$W = \overline{V}(\infty) - E_F,$$

where $\overline{V}(\infty)$ is the plane-averaged electrostatic potential in the vacuum at a distance where the microscopic potential has reached its asymptotic value and E_F is the Fermi energy.

The electrostatic potential $V(x,y,z)$ on a grid in real space can be obtained from a self-consistent electronic structure calculation using a plane wave basis set. Assuming that the surface normal is oriented along the *z*-axis, one can define a plane averaged potential:

$$\overline{V}(z) = \frac{1}{A}\iint_{cell} V(x,y,z)dxdy$$

where A is the supercell surface area. The asymptotic value $\overline{V}(\infty)$ can be extracted by plotting the variation of $\overline{V}$ as a function of z. Simple electrostatics gives the relation between the change in work function and the change in surface dipole[30]

$$\Delta W = \frac{e\Delta\mu}{\epsilon_0 A_{atom}}$$

where A_{atom} is the surface area taken up by one adatom, ϵ_0 is the electric permittivity of free space and $\Delta\mu$ is the change in surface dipole that occurs upon atomic adsorption, normalized per adatom. $\Delta\mu$ corresponds to the z-component of the dipole moment directed along the surface normal, since only this component affects significantly the work function.

It should be noted that the major contribution to the surface dipole results from the charge reordering associated with the formation of the chemical bonds between the metal surface and the adatoms. This contribution is foremost determined by the nature of the chemical bonds, but can also be modified by the packing density of the adatoms.

3 Results and discussion

3.1 Adsorption of Cs on graphene

In this section, the adsorption of Cs atoms on free-standing MLG and BLG and the changes in work function upon Cs adsorption are investigated.

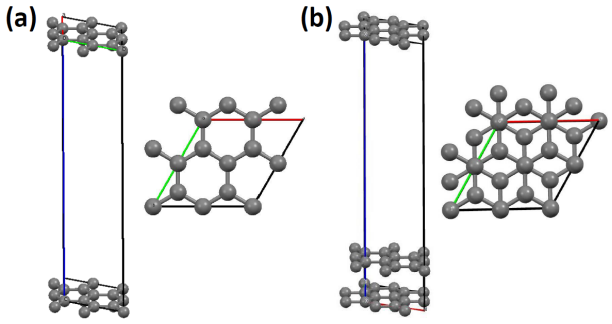

Fig. 1 Crystal supercells of (2×2) (a) monolayer graphene and (b) bilayer graphene. Geometries were relaxed at the LDA/CA level of theory. Color legend: C, grey.

The structures of the (2×2) MLG and BLG supercells relaxed at the LDA/PWC level of theory are depicted in Figure 1. For MLG, the structural lattice parameters obtained at the LDA/PWC

level were found to be: $a = b = 4.89$ Å (with a vacuum layer along the z-axis fixed to 20 Å), $\alpha = \beta = 90°$, $\gamma = 120°$. The lattice parameters relaxed at the GGA/PBE and GGA/PW91 levels of theory resulted in $a = b = 4.94$ Å and $a = b = 4.93$ Å, respectively. These values are in good overall agreement with experimental lattice parameters for graphite: $a = b = 4.912$ Å (c =6.696 Å), $\alpha = \beta = 90°$, $\gamma = 120°$.[31] As expected, experimental lattice parameters are slightly larger (smaller) than the values calculated with LDA (GGA), due to the well-known overbinding (underbinding) character of LDA (GGA). The plane-averaged electrostatic potential in the vacuum, $\overline{V}(\infty)$, of MLG was found to be 1.55 eV for LDA/PWC, 1.50 eV for GGA/PBE and 1.51 eV for GGA/PW91. The Fermi energy, E_F, of MLG was calculated to be -3.82 eV for LDA/PWC, -3.60 eV for GGA/PBE and -3.64 eV for GGA/PW91. As a result, the computed work function, W, of MLG was: 5.37 eV for LDA/PWC, 5.10 eV for GGA/PBE, and 5.15 eV for GGA/PW91. These values appear slightly larger than the value of *ca*. 4.66 eV determined experimentally for MLG.[32] Unless otherwise stated, all the subsequent calculations were carried out using LDA/PWC.

For BLG, similar structural parameters as in the case of MLG were obtained with LDA/PWC: $a = b = 4.89$ Å, with an optimized interlayer spacing of 3.18 Å, and $\alpha = \beta = 90°$, $\gamma = 120°$. Let us note that the computed interlayer spacing of BLG is slightly shorter than the distance $c/2 = 3.348$ Å in graphite with graphene layers periodically stacked with a Bernal sequence. The plane-averaged electrostatic potential in the vacuum was found to be $\overline{V}(\infty) = 3.11$ eV for LDA/PWC, with the Fermi energy $E_F = -1.95$ eV, resulting in a work function of 5.06 eV.

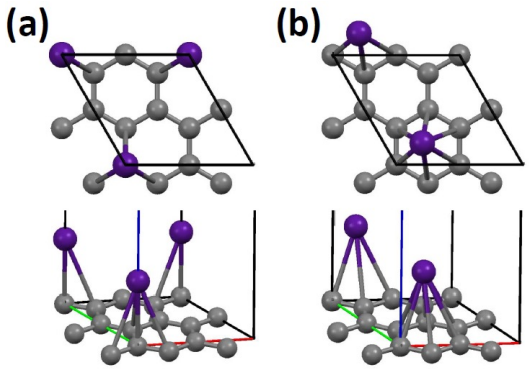

Fig. 2 Crystal supercells of Cs adsorption on a (2×2) graphene monolayer at (a) atop sites and (b) hollow sites. Geometries were relaxed at the LDA/PWC level of theory. Color legend: C, grey; Cs, purple.

The relaxed structures for one Cs atom adsorption on the (2×2) MLG calculated at the LDA/PWC level of theory are show in Figure 2. Cs atom adsorption at "atop" sites and "hollow" sites were investigated for a 1:8 coverage ratio of Cs/C atoms. For adsorption of Cs atoms at atop sites, the computed bond distances were d(Cs–C) = 3.01 and 3.30 Å and correspond to a Cs binding energy of $E_B = 0.56$ eV. For adsorption of Cs atoms at hollow sites, the average bond distance was d(Cs–C) = 3.27 Å and corresponds to a Cs binding energy of $E_B = 0.63$ eV. Therefore, Cs adsorption at the hollow sites is predicted to be more energetically favorable by 0.07 eV than at atop sites. The predicted $\overline{V}(\infty)$ values were 1.45 and 1.69 eV for Cs adsorption at atop and hollow sites, respectively, with a corresponding Fermi energy value of -0.68 eV in both cases. The resulting work function W is 2.13 and 2.37 eV for adsorption at atop and hollow sites, respectively. Therefore, the change in work function, ΔW, upon adsorption of a Cs atom on the (2×2) MLG is 3.24 eV for adsorption at atop sites and 3.00 eV for adsorption at hollow sites.

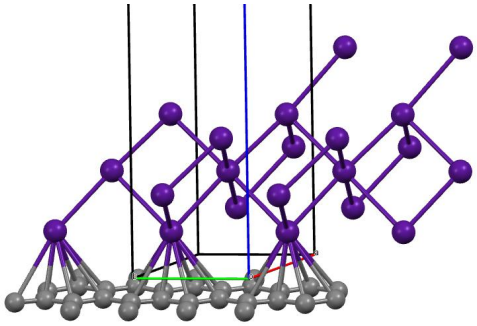

Fig. 3 Crystal supercell of Cs adsorption on (2×2) graphene monolayer, with a 4:8 coverage ratio of Cs/C atoms, relaxed at the LDA/CA level of theory. Color legend: C, grey; Cs, purple.

Structural optimization of Cs-MLG was also investigated for a 4:8 coverage ratio of Cs/C atoms, with all the Cs atoms occupying hollow sites. However, it was found that only a limited number of Cs atoms were adsorbed and a tendency to form multilayer-thick Cs cubic structures from the Cs atoms that desorbed was observed (see, e.g., Figure 3). Such situations are likely to be encountered when the Cs pressure in the trap is increase, leading possibly to epitaxial growth of a Cs thin film on the MLG substrate. If this is the case, the change in work function would be expected to correspond to the difference in work function between MLG and bulk Cs.

The relaxed structures for one Cs atom adsorption on the (2×2) BLG calculated at the LDA/PWC level of theory are shown in Figure 4, with Cs atom adsorption at atop and hollow sites (1:8 coverage ratio of Cs/C atoms). The calculated Cs binding energies on BLG are identical to the case of Cs adsorption on MLG, i.e. $E_B = 0.56$ eV for Cs at atop sites and $E_B = 0.63$ eV for Cs at hollow sites. The computed bond distances were d(Cs–C) = 2.97 and 3.26 Å for Cs adsorption at atop sites and the average bond distance was d(Cs–C) = 3.23 Å for Cs adsorption at hollow sites.

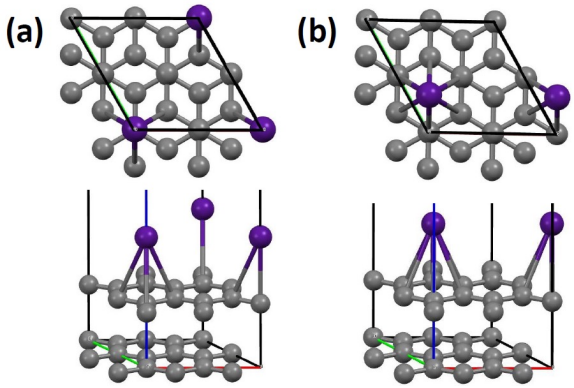

Fig. 4 Crystal supercells of Cs adsorption on a (2×2) graphene bilayer at (a) atop sites and (b) hollow sites. Geometries were relaxed at the LDA/CA level of theory. Color legend: C, grey; Cs, purple.

The $\overline{V}(\infty)$ values were 2.88 and 2.96 eV for Cs adsorption at atop and hollow sites, respectively, with a corresponding Fermi energy value of 0.70 eV for Cs atop-site adsorption and 0.57 eV for Cs hollow-site adsorption. The resulting work function W is 2.18 and 2.39 eV for adsorption on BLG at atop and hollow sites, respectively; only small variations are predicted with regard to the values of 2.13 and 2.37 eV for adsorption on MLG at atop and hollow sites. Therefore, the change in work function, ΔW, upon adsorption of a Cs atom on the (2×2) BLG is 2.88 eV for adsorption at atop sites and 2.67 eV for adsorption at hollow sites. These changes in work function are slightly smaller than in the case of adsorption on a MLG (3.00 and 3.24 eV for hollow and atop adsorption, respectively), thus suggesting the formation of a smaller dipole moment created by the adatoms on BLG compared to MLG.

3.2 Adsorption of Cs on graphene-veiled SiO_2

In this section, the adsorption of Cs atoms on graphene-veiled $SiO_2(0001)$ surfaces is investigated for both MLG and BLG covering $SiO_2(0001)$.

The trigonal crystal unit cell of bulk α-quartz (SiO_2; space group $P3_221$, IT No. 154) was relaxed at the LDA/PWC level of theory (cf. Figure 5). The optimized lattice parameters were $a = b = 4.91$ Å, $c = 5.40$ Å, $\alpha = \beta = 90°$, $\gamma = 120°$. These values are in excellent agreement with the diffraction measurements of Levien and co-workers,[33] i.e. $a = b = 4.916$ Å, $c = 5.4054$ Å, $\alpha = \beta = 90°$, $\gamma = 120°$.

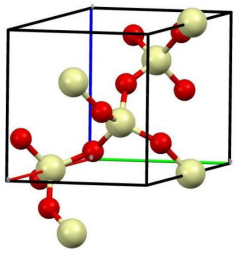

Fig. 5 The trigonal crystal unit cell of bulk α-quartz (SiO_2; space group $P3_221$, IT No. 154) relaxed at the LDA/PWC level of theory. Color legend: O, red; Si, yellow.

As shown in Figure 6, O- and Si- terminated $SiO_2(0001)$ surfaces were built by cleaving the relaxed bulk structure of α-quartz (Figure 5) and consisted of 5 and 6 bilayer of SiO_2, with the back side of the slabs passivated by addition of hydrogen atoms; a large vacuum region of *ca*. 20 Å was used between periodic slabs.

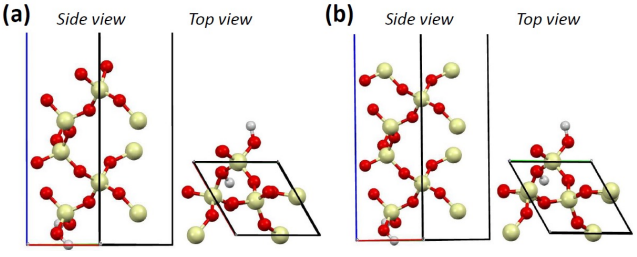

Fig. 6 Crystal supercells of $SiO_2(0001)$ slabs with (a) O-atom termination and (b) Si-atom termination. The back side of the slabs was passivated by addition of hydrogen atoms. Geometries were relaxed at the LDA/PWC level of theory. Color legend: O, red; Si, yellow; H, hydrogen.

For the clean O-terminated $SiO_2(0001)$ surface, the vacuum potential $\overline{V}(\infty)$ was found to be 4.29 eV and the Fermi-level energy was -5.33 eV, resulting in a work function of 9.62 eV. For Si-terminated $SiO_2(0001)$ surface, $\overline{V}(\infty)$ was calculated to be 3.76 eV and the Fermi energy -2.83 eV, thus the predicted work function was 6.59 eV, significantly lower than for the O-terminated quartz surface.

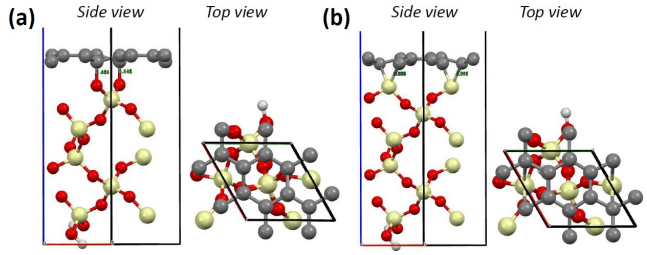

Fig. 7 Crystal supercells of (2×2) MLG-veiled $SiO_2(0001)$ slabs with (a) O-atom termination and (b) Si-atom termination. The back side of the slabs was passivated by addition of hydrogen atoms. Geometries were relaxed at the LDA/PWC level of theory. Color legend: O, red; Si, yellow; H, hydrogen.

The optimized structures of O- and Si-terminated $SiO_2(0001)$ slabs covered with one MLG calculated at the LDA/PWC level are displayed in Figure 7. The computed bond distances were d(C–O) = 1.45–1.46 Å and d(C–Si) = 2.06–2.10 Å for O- and Si-terminated slabs, respectively. The binding energy of the (2×2) MLG to O-terminated $SiO_2(0001)$ is about 3.20 eV and about 1.28 eV to Si-terminated $SiO_2(0001)$. For the (2×2) MLG-veiled $SiO_2(0001)$ slab with O-atom termination, $\overline{V}(\infty) = 3.63$ eV and E_F= -2.57 eV, thus the predicted work function W is 6.20 eV. Therefore, the addition of a MLG changes the work function of the clean O-terminated surface by $\Delta W = 3.42$ eV. For the (2×2) MLG-veiled $SiO_2(0001)$ slab with Si-atom termination, $\overline{V}(\infty) = 4.84$ eV and E_F = -0.28 eV, resulting in a smaller work function of W = 5.12 eV. The addition of a MLG changes the work function of the Si-terminated surface by only $\Delta W = 1.47$ eV. This smaller change in work function upon covering the Si-terminated $SiO_2(0001)$, relative to the O-terminated quartz surface, is expected due to the weaker C–Si bonding compared to the strong C–O bonding [see above, d(C–O) < d(C–Si)]. Let us note that, under normal atmospheric conditions, O-terminated $SiO_2(0001)$ will be predominant relative to Si-terminated $SiO_2(0001)$. Therefore, we will focus on modelling O-terminated $SiO_2(0001)$ throughout the rest of this study.

The optimized structures for the adsorption of Cs at hollow sites of (2×2) MLG-veiled and BLG-veiled $SiO_2(0001)$ slabs with O-atom termination are depicted in Figures 8 and 9, respectively.

Three locations were studied for the adsorption of Cs at hollow sites of a (2×2) MLG-veiled $SiO_2(0001)$ slab [Figure 8(a)–(c)]. The computed bond distances d(Cs–C) were all in the range 3.25–3.33 Å with the presence of four to six bonds. The computed binding energies were: (a) 0.54 eV; (b) 0.67 eV; (c) 0.52 eV. These values are close to the value of $E_B = 0.63$ eV for Cs adsorption at hollow sites on a free-standing MLG. The predicted $\overline{V}(\infty)$ and E_F values were, respectively: (a) 3.02 and 0.81 eV; (b) 3.23 and 0.70 eV; (c) 3.07 and 0.83 eV. Therefore,

the corresponding work functions were: (a) 2.21 eV; (b) 2.53 eV; (c) 2.24 eV. In turn, the change in work function ΔW as a result of Cs adsorption at these three locations was: (a) 3.99 eV; (b) 3.67 eV; (c) 3.96 eV. These ΔW values are slightly larger than in the case of the adsorption of a Cs atom at hollow sites on the free-standing (2×2) MLG, i.e. ΔW = 3.00 eV. This means that larger adatom-surface dipole moments are created when a MLG-veiled quartz substrate is used compared to the adsorption on MLG alone.

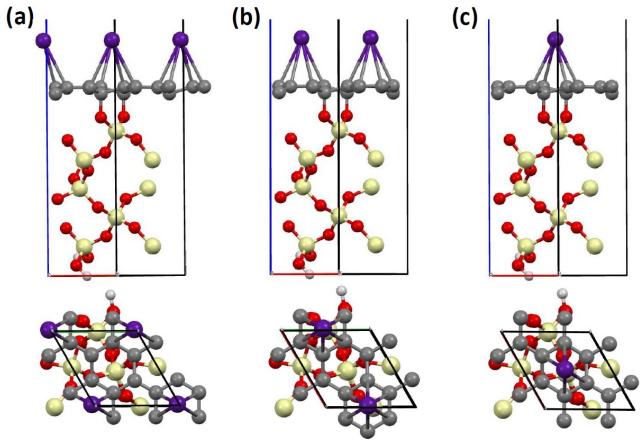

Fig. 8 Optimized structures for the adsorption of Cs at hollow sites of a (2×2) MLG-veiled SiO_2(0001) slab with O-atom termination. Geometries were relaxed at the LDA/PWC level of theory. Color legend: O, red; Si, yellow; H, hydrogen; Cs, purple.

The optimized structures of a clean (2×2) BLG-veiled SiO_2(0001) slab and for the three possible adsorption sites of Cs at hollow sites of a (2×2) BLG-veiled SiO_2(0001) slab with O-atom termination are shown in Figure 9. For the clean BLG-veiled SiO_2(0001) slab [Figure 9(a)], the interlayer spacing for the BLG ranges between 3.11 and 3.48 Å, due to the buckling of the bottom graphene sheet as a result of the strain created by the formation of C–O covalent bonds and the slight lattice mismatch between the (2×2) graphene and the SiO_2(0001) surface. This interlayer spacing is in line with the value of 3.18 Å calculated for a free-standing BLG and the value of 3.348 Å determined experimentally for graphite. For the clean BLG-veiled SiO_2(0001) slab, the predicted $\overline{V}(\infty)$ and E_F values were 4.53 and -0.91 eV, respectively, thus resulting in a work function of 5.44 eV. This work function is slightly larger than the value of 5.06 eV for the free-standing BLG, therefore suggesting the occurrence of charge transfer between the BLG and the SiO_2(0001) surface.

The Cs adsorption at three different hollow sites of the (2×2) BLG-veiled SiO_2(0001) slab [Figure 9(b)–(c)] has been investigated. The computed Cs–C bond distances were all in the range 3.22–3.24 Å with the presence of six bonds per Cs atom; this contrasts with the case of Cs adsorption on GML where Cs exhibited both four- and six-fold coordination to the graphene sheet. The calculated binding energies for (b)–(c) are essentially degenerate with a value of E_B = 0.65 eV, in contrast to Cs adsorption on the MLG-veiled SiO_2(0001) which featured adsorption energies between 0.52 and 0.67 eV.

The computed $\overline{V}(\infty)$ and E_F values were, respectively: (b) 4.02 and 1.52 eV; (c) 4.00 and 1.51 eV; (d) 4.02 and 1.52 eV. This leads to work function values of (b) 2.50 eV, (c) 2.49 eV, (d) 2.50 eV, and, therefore, a nearly identical change in work function of around ΔW = 2.94 eV as a result of Cs adsorption at these three locations shown in Figure 9. This value is comparable to the ΔW = 3.00 eV obtained for adsorption of a Cs atom at hollow sites on the free-standing (2×2) MLG, while significantly smaller than the values of 3.67-3.99 eV for the adsorption of Cs at hollow sites of a (2×2) MLG-veiled SiO_2(0001) slab. This, again, suggests the formation of smaller dipole moments created by the adatoms on BLG compared to MLG.

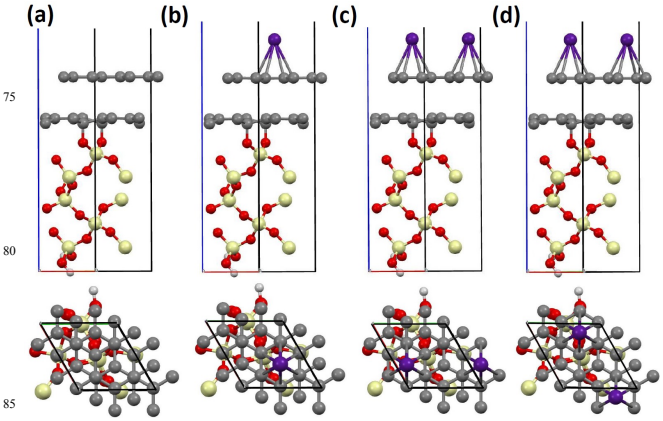

Fig. 9 Optimized structures for the adsorption of Cs at hollow sites of a (2×2) BLG-veiled SiO_2(0001) slab with O-atom termination. (a) clean (2×2) BLG-veiled SiO_2(0001) slab; (b)–(d) possible geometries for Cs adsorption. Geometries were relaxed at the LDA/PWC level of theory. Color legend: O, red; Si, yellow; H, hydrogen; Cs, purple.

Conclusions

In summary, atomistic calculations aimed at studying the interactions of Cs atoms with mono- or bi-layered graphene, either free-standing or placed on a SiO_2 substrate, have been reported. The most stable adsorption sites for Cs are found to be hollow sites on graphene and the corresponding binding energies, Fermi energies, asymptotic plane-averaged electrostatic potentials in the vacuum, work functions and changes in work function have been systematically calculated. The most stable adsorption sites were found to be at hollow sites of the graphene sheets. It was also found that larger dipole moments are created when a MLG-veiled SiO_2(0001) substrate is used for the adsorption of Cs atoms compared to the adsorption on a free-standing MLG alone, due to charge transfer occurring between the MLG and the quartz substrate. For the adsorption on MLG-veiled SiO_2(0001) substrate, preferential Cs adsorption sites appear among the allow sites, as a result of the strong covalent bonding of the MLG to quartz. However, for the adsorption of Cs on BLG-veiled SiO_2(0001) substrate, these differences are smoothed out and the binding energies corresponding to different sites are nearly degenerate; smaller dipole moments created by the Cs adatoms on BLG compared to MLG are also predicted.

Further DFT calculations will investigate the interaction potentials at various distances between the Cs adatoms and the different MLG and BLG free-standing and veiled SiO_2(0001) surfaces and predict the jitter noise in these systems.

Acknowledgments. Sandia National Laboratories is a multi-program laboratory managed and operated by Sandia Corporation, a wholly owned subsidiary of Lockheed Martin Corporation, for the U.S. Department of Energy's National Nuclear Security Administration under contract DE-AC04-94AL85000.

Notes and references

[a] *Sandia National Laboratories, Albuquerque, NM 87185, USA. E-mail: pfweck@sandia.gov*
[b] *Department of Physics and Astronomy, University of Nevada Las Vegas, Las Vegas, NV 89154, USA.*

[1] I. Langmuir, K. H. Kingdon, *Phys. Rev.,* 1923, **21**, 380.
[2] I. Langmuir, *J. Am. Chem. Soc.,* 1932, **54**, 2798.
[3] R. W. Gurney, *Phys. Rev.,* 1935, **47**, 2798.
[4] W. N. Unertl, *Physical Structure*, Handbook of Surface Science, vol. 1., N. V. Richardson, S. Holloway, Eds., North-Holland, Elsevier, Amsterdam, 1996
[5] A. Laliotis, T. Passerat de Silans, I. Maurin, M. Ducloy, D. Bloch, *Nature Comm*., 2014, **5**, 4364.
[6] G. Ertl, in *The Physics and Chemistry of AM Adsorption*, H. P. Bonzel, A. M. Bradshaw, G. Ertl, Eds., Elsevier, Amsterdam, 1989.
[7] W. Mross, *Catal. Rev. Sci. Eng.*, 1983, **25**, 591.
[8] J. M. McGuirk, D. M. Harber, J. M. Obrecht, E. A. Cornell, *Phys. Rev.* A*,* 2004, **69**, 062905.
[9] A. Safavi-Naini, P. Rabl, P. F. Weck, H. R. Sadeghpour, *Phys. Rev.* A*,* 2011, **84**, 023412.
[10] A. Safavi-Naini, E. Kim, P. F. Weck, P. Rabl, H. R. Sadeghpour, *Phys. Rev.* A*,* 2013, **87**, 023421.
[11] Y. M. Lin, P. Avouris, *Nano Letters,* 2008, **8**, 2119.
[12] M. Ishigami, J. H. Chen, W. G. Cullen, M. S. Fuhrer, E. D. Williams, *Nano Letters*, 2007, **7**, 1643.
[13] H. Kim, I. Song, C. Park, M. Son, M. Hong, Y. Kim, J. S. Kim, H. J. Shin, J. Baik, H. C. Choi, *ACS Nano*, 2013, **7**, 6575.
[14] D. Q. McNerny, B. Viswanath, D. Copic, F. R. Laye, C. Prohoda, A. C. Brieland-Shoultz, E. S. Polsen, N. T. Dee, V. S. Veerasamy, A. J. Hart, *Sci. Rep*., 2014, **4**, 5049.
[15] Y. J. Kang, J. Kang, K. J. Chang, *Phys. Rev.* B, 2008, **78**, 115404.
[16] P. Shemella, S. K. Nayak, *App. Phys. Lett*., 2009, **94**, 032101.
[17] P. Jadaun, S. K. Banerjee, L. F. Register, B. Sahu*, J. Phys.: Condens. Matter*, 2011, **23**, 505503.
[18] P. Jadaun, B. R. Sahu, L. F. Register, S. K. Banerjee*, Sol. State Comm.*, 2012, **152**, 1497.
[19] M. Caragiu, S. Finberg, *J. Phys.: Condens. Matter*, 2005, **17**, R995.
[20] G. Kresse, J. Furthmüller, *Phys. Rev.* B, 1996, **54**, 11169.
[21] J. P. Perdew, Y. Wang, *Phys. Rev. B,* 1996, **45**, 13244.
[22] J. P. Perdew, K. Burke, M. Ernzerhof , *Phys. Rev. Lett.*, 1996, **77**, 3865.
[23] J. P. Perdew, J. A. Chevary, S. H. Vosko, K. A. Jackson, M. R. Pederson, D. J. Singh, C. Fiolhais, *Phys. Rev.* B, 1992**, 46**, 6671.
[24] P. E. Blöchl, *Phys. Rev.* B, 1994, **50**, 17953.
[25] G. Kresse, D. Joubert, *Phys. Rev.* B, 1999, **59**, 1758.
[26] E. R. Davidson, *Methods in Computational Molecular Physics*, G. H. F. Diercksen and S. Wilson, Eds., Vol. 113, NATO Advanced Study Institute, Series C, Plenum, New York, 1983, p. 95.
[27] M. Methfessel, A. T. Paxton, *Phys. Rev.* B, 1989, **40**, 3616.
[28] H. J. Monkhorst, J. D. Pack, *Phys. Rev.* B, 1976, **13**, 5188.
[29] J. Neugebauer, M. Scheffler, *Phys. Rev.* B, 1992, **46**, 16067.
[30] J. D. Jackson, *Classical Electrodynamics*, Wiley, New York, NY, 1975.
[31] R. W. G. Wyckoff, *Crystal Structures*, vol. 1, second edition. Interscience Publishers, New York, NY, 1963
[32] Y. Shi, K. K. Kim, A. Reina, M. Hofmann, L. Li, J. Kong, *ACS Nano,* 2010, **4**, 2689.
[33] L. Levien, C. T. Prewitt, D. J. Weidner, *Am. Miner.*, 1980, **65**, 920.

